HYDROGEN, FUEL CELL & ENERGY STORAGE

Thermoeconomic Analysis and Optimization of a Novel Geothermal Energy-Based Multigeneration System for Liquid Hydrogen, Hot Water, Cooling and Power Production

Ali Eyvazi[a,*] | **Mehran Ameri**[b] | **Mohammad Shafiey Dehaj**[a] | **Hadi Ghaebi**[c]

[a] Department of Mechanical Engineering, Faculty of Engineering, Vali-e-Asr University of Rafsanjan, Rafsanjan, Iran
[b] Department of Mechanical Engineering, Faculty of Engineering, Shahid bahonar University of Kerman, Kerman, Iran
[c] Department of Mechanical Engineering, Faculty of Engineering, University of Mohaghegh Ardabili, Ardabil, Iran
[*] Corresponding author, Email: alieyvazi1996@gmail.com

Article Information

Article Type
Research Article

Article History
Received: *02 Nov 2025*
Revised: *20 Dec 2025*
Accepted: *16 Feb 2026*
Published Online: *08 Mar 2026*

Keywords
Geothermal energy
Claude hydrogen liquefaction cycle
Multigeneration system
Optimization
Modified organic rankine cycle

Abstract

This study examines a sustainable energy framework designed for hydrogen production. It includes various components like a geothermal energy module, a Claude cycle system for hydrogen liquefaction, and a modified organic Rankine cycle. A detailed investigation into its operational features is conducted across various aspects, with its energy conversion efficiency measured using key performance indicators. The assessment of operational effectiveness was based on factors such as energy yield, exergy utilization, and economic considerations. A sensitivity analysis assesses how changes in operation affect performance. A dual-objective genetic algorithm with the TOPSIS method enhances the hydrogen production infrastructure. The system achieves an energy conversion efficiency of 45% and exergy efficiency of 53%, producing 4.88 kg of hydrogen per hour and 1,425 kW of power, with operational costs of $37.16 per hour. The Levelized Cost of Energy is 19.8 cents per kWh, while the Levelized Cost of Hydrogen is 24.39 $/kg. The energy needed for hydrogen liquefaction is reduced through a two-stage thermal management strategy.

Cite this article: Eyvazi, A., Ameri, M., Shafiey Dehaj, M., Ghaebi, H. (2026). Thermoeconomic Analysis and Optimization of a Novel Geothermal Energy-Based Multigeneration System for Liquid Hydrogen, Hot Water, Cooling and Power Production. DOI: 10.22104/hfe.2025.7627.1362

 Publisher: Iranian Research Organization for Science and Technology (IROST)
DOI: 10.22104/hfe.2025.7627.1362

1 Introduction

The growth of cities and the increasing need for energy have led experts to focus on creating reliable energy solutions. Discussions on energy efficiency must consider cost and environmental care [1]. Combined Heat and Power (CHP) systems, or cogeneration, are important in decentralized energy production. They produce multiple types of useful energy from one fuel source, improving efficiency and reducing fuel use and pollution. Current methods waste much energy as low-grade heat, making it vital to recover these resources for better overall efficiency [2]. There is a strong need for energy optimization and sustainable energy due to limited fossil fuels and environmental harm. Combined heat and power (CHP) technology effectively meets energy demands and offers financial benefits [3]. Efficiency is crucial due to the rising costs of fossil fuels, their limited availability, and environmental issues. Adopting alternative energy, especially renewables like geothermal energy, is vital for stable power from the Earth's heat. Geothermal energy is useful for heating, cooling, drying, and distillation, depending on source characteristics [4]. The Earth contains a vast, hidden energy source from the sun, known as geothermal energy, which can meet current and future energy needs if accessed correctly [5].

Geothermal energy comes from the heat inside the Earth, with temperatures increasing as depth increases. Heat moves from hot areas to cooler ones, leading to high-temperature reservoirs in certain geological zones that can be used for energy [6]. This approach generates energy without fuel, similar to wind and solar power, helping to save fossil resources and keep the air clean. The environmental impact of geothermal energy is now very low due to re-injecting fluids back into the earth. These facilities take up less land and avoid many problems other energy sources face. They operate continuously, even in tough conditions [7]. Hydrogen is emerging as a highly advantageous energy transfer medium due to its storage versatility, high energy density, and zero emissions when combusted. It holds potential for various applications, including vehicle propulsion, heating, and decentralized electricity generation, especially in remote areas. Economically and logistically, hydrogen may be more appealing than traditional electrical power, fueling research for its integration into societal energy needs [8]. Hydrogen, a sustainable alternative to fossil fuels, faces challenges due to low volumetric density, complicating transport and storage. Liquefaction is key for enhancing its energy density. Supported by advancements in fuel cell technology, hydrogen's role in renewable energy systems as a clean and enduring power source is increasingly recognized [9, 10].

A groundbreaking liquid hydrogen generation apparatus was unveiled by Bi et al. [11], who then contrasted its operational metrics with predecessor designs. They evaluated its inherent thermodynamic imperfections by quantifying the exergy detriment associated with each distinct section of the system. This new development recorded an 18% performance factor and a 54% exergy efficiency. The study conducted by Kaykha and colleagues [12] centered on refining a geothermal infrastructure that incorporated organic Rankine cycles, dual-stage and dual-pressure evaporation practices, and zeotropic fluid mixtures. Their subsequent analysis demonstrated that the most substantial systemic energy hemorrhage originated from the steam turbine and its corresponding expansion valve, rendering them the greatest sources of wasted power. Separately, Cao et al. [13] engineered a synergistic system combining solar and geothermal energy, strategically designed to meet the power requirements of urban environments and decrease running costs by exporting excess electricity back to the main utility grid.

Mehrpoya et al. [14] devised an innovative approach for the simultaneous liquefaction of both hydrogen and natural gas. Their proposed system featured a distinctive configuration employing a multi-component refrigerant, achieving an exergy efficiency of 0.24 and a coefficient of performance (COP) of 62.54%. Separately, Zoo et al. [15] explored coupling a wind-powered cogeneration system with a hydrogen generation facility. They reported that incorporating larger wind turbines led to enhanced economic outcomes, superior energy utilization, and a diminished carbon dioxide footprint. Siam et al. [16] engineered a substantial, large-scale system incorporating a cloud cycle and a nitrogen pre-cooling unit. This design, powered by three 130 MW isobutane power plants, demonstrated a daily production capacity of 335 metric tons and significantly reduced the specific electricity consumption during liquefaction by 6.41 kWh/kg. Separately, Nouri et al. [17] unveiled a system capable of simultaneously producing liquid hydrogen and carbon dioxide. Leveraging photovoltaic and electrolysis technologies, their setup achieved an hourly output of 3.3 kg of liquid hydrogen and 10.4 kg of liquid carbon dioxide. Studies focused on enhancing cryogenic processes have yielded several key findings.

Ho Myung et al. [18], for instance, focused their research on a specialized liquefaction configuration, finding that incorporating a Liquefied Natural Gas (LNG) cooling module improved the overall operational efficacy of the system. Extending this area of research, Teknat and colleagues [19] provided evidence that replacing conventional nitrogen with LNG dur-

ing the hydrogen precooling sequence generates substantially greater efficiency within the observed architecture. Their findings specified compelling thermodynamic results: the studied system attained an energy efficiency of 51.53%, alongside an exergy efficiency of 59.17%. This drive toward highly optimized, advanced power systems is essential in the current climate, spurred by both the escalation of energy expenditures globally and the pressing environmental mandate to mitigate global warming through solutions that maximize efficiency and drastically curtail emissions. Given the constrained availability of sustainable power, methodologies involving the integration of distinct energy systems have been explored specifically for the purpose of reclaiming thermal energy that would otherwise be discarded. This particular investigation focuses on utilizing the residual heat discharged by an adapted Rankine power cycle – which acts as the foundational energy structure – to drive the synthesis of hydrogen. This strategy is highly effective because the temperature characteristics of the Rankine system's exiting streams are optimally matched to the thermal input requirements of the downstream hydrogen generation process. Harnessing a single process to yield multiple valuable outputs simultaneously offers significant advantages, proving economically sound, energetically efficient, and broadly effective.

Acknowledging the extensive prior advancements in system design, this research introduces a novel integrated thermodynamic cycle. This innovative framework is specifically engineered for the parallel generation of both electrical power and hydrogen. Its foundational structure modifies a conventional Rankine system, with the key distinction and original contribution of this study being the seamless incorporation of a Proton Exchange Membrane (PEM) electrolyzer and a dedicated Claude liquefaction system for hydrogen. The core purpose of this investigation is to thoroughly analyze the entire system from both a thermodynamic and thermoeconomic perspective. This will be accomplished using the EES software, alongside a comprehensive parametric investigation. A novel advancement aimed at mitigating environmental impacts involves the seamless integration of a PEM electrolyzer, which capitalizes on the surplus thermal energy from a modified Rankine system to simultaneously generate both electricity and hydrogen.

2 System Description

Detailed in Figure 1 is the conceptual layout of the geothermal energy system central to this study. Its operational architecture brings together a hydrogen liquefaction Claude cycle, an absorption precooling cycle, a modified organic Rankine cycle, a geothermal power unit for energy provision, and an electrolyzer for generating hydrogen through water electrolysis. To achieve superior operational effectiveness, the configuration of the Organic Rankine Cycle (ORC) apparatus was significantly upgraded through the simultaneous integration of an internal thermal recovery unit and a generator linked to a steam-fed heat exchange mechanism. These modifications function alongside the foundational machinery of the system: the expander, the vaporizer, the heat sink, and the fluid pressurizer. Immediately after the high-temperature subterranean working fluid exits the pressure-regulating throttling device, it is directed onward into the separation chamber.

Steam is directed to Turbine 1, whereas the liquid phase is handled by the Organic Rankine Cycle (ORC) heat exchanger. This ORC employs a fluid with a low boiling point, enabling its evaporator to produce vapor for Turbine 2 from modest heat sources. After passing through Turbine 2, the working fluid is cooled and liquefied in Condenser 2, then returned to the system by the pump. Operational efficacy is boosted within the Organic Rankine Cycle (ORC) by integrating an internal heat recovery unit. This regenerator works to minimize thermal dissipation typically occurring in the condenser by channeling the waste heat from the turbine's exhaust to preheat the pressurized working fluid exiting the pump. Concurrently, the output stream generated by Turbine 1 supplies the input flow to the electrolyzer.

The overall process initiates with a single-effect absorption chiller subjecting the electrolytic hydrogen to preliminary cooling, a tactical step that dramatically curtails the subsequent energetic requirements necessary for conversion into liquid form. Submitting to a Claude cycle compressor, the hydrogen is subsequently divided into two distinct streams. The initial stream undergoes cooling within Heat Exchanger 1, which employs chilled vapor sourced from a separator. Simultaneously, Heat Exchanger 2 leverages nitrogen gas to cool the second, parallel hydrogen stream. These two flows then converge before proceeding into a precooler, which is immersed in a bath of liquid nitrogen. Further thermal reduction is achieved in an additional heat exchanger using separator-derived vapor, preceding the hydrogen's departure from the system. Once separated from its gaseous phase, the produced liquid hydrogen is then meticulously stored in a reservoir. The essential energy input for this system is drawn from a subterranean geothermal facility, which extracts thermal energy stored within the Earth's crust. System efficiency is significantly boosted through an integrated steam thermal exchange unit that recovers

excess waste heat, optimizing the performance of the adapted Rankine thermodynamic circuit. The resulting process generates gaseous dihydrogen and dioxygen via Proton Exchange Membrane (PEM) electrochemical decomposition of water. An Organic Rankine Cycle (ORC) generator delivers the requisite consistent and carbon-neutral electrical current that powers the electrolysis, thereby facilitating the sustained and environmentally sound production of hydrogen. Following this, a Claude refrigeration process is employed to convert the gaseous hydrogen, previously produced through electrolysis, into its liquid state. This liquefaction greatly streamlines both its containment and distribution. Beyond its core function of hydrogen generation, this geothermal-powered infrastructure also provides essential thermal regulation services, encompassing both heating and cooling. The strategic selection of R123 as the zeotropic working fluid for the Organic Rankine Cycle (ORC) significantly enhances the system's overall efficiency and reinforces its commitment to environmental stewardship, primarily due to R123's negligible ecological impact, exceptional thermodynamic performance, and cost-effective applicability.

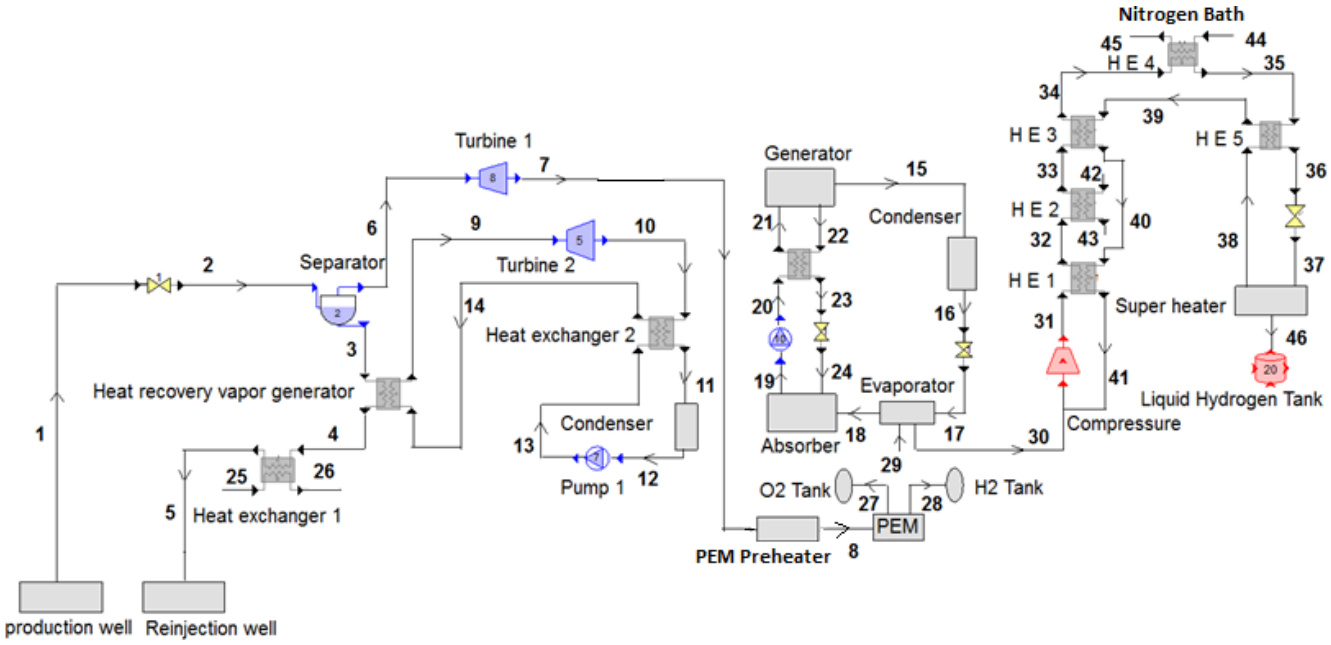

Fig. 1. Schematic view of the proposed system

The evaluated system is modeled using the following presumptions [20]:

- Every system component takes the steady-state condition into account.
- The reference conditions, 101 kPa for pressure and 20 °C for temperature, are applied.
- Kinetic and potential energies are excluded from the system's performance analysis.
- The performance of compressors, turbines, and pumps is characterized by their isentropic efficiencies.

3 Thermodynamic Modeling of the System

Energy and exergy assessments are crucial for studying energy transformation systems. Traditional energy analysis overlooks the qualitative differences among energy forms, while exergy analysis evaluates their true utility based on thermodynamic principles. This approach identifies inefficiencies and wasted energy, creating a robust framework for thermodynamic evaluation. The goal is to enhance energy and exergy efficiency while reducing exergy dissipation. The governing equations are systematically applied to every steady-state control volume within the system [21]:

$$\sum m_i = \sum m_e \,, \tag{1}$$

$$Q - W = \sum m_e h_e - \sum m_i h_i \,. \tag{2}$$

$\dot{m}$ denotes the mass flow rate, Q the heat exchange rate within the control volume, and W the work exchange rate. Energy, a fundamental capacity for change or work, is governed by conservation principles, outlined

in the First Law of Thermodynamics. This law recognizes energy as a primary thermodynamic attribute, manifesting either as intrinsic content or as an exchange through specific pathways. The Second Law of Thermodynamics introduces a hierarchy, asserting energy's inherent quality diminishes during natural processes, evidenced by thermal energy migration from high to low temperatures. It emphasizes an increase in total entropy, illustrating thermodynamic irreversibility. Consequently, exergy analysis identifies inefficiencies within thermodynamic systems, enabling improvements in both operational modes and efficiency by pinpointing areas where energy potential is wasted. This method, in essence, provides the conceptual basis for computing specific physical exergy [21]:

$$\mathrm{ex}_{\mathrm{ph}} = (h - h_0) - T_0(s - s_0) \tag{3}$$

The specific enthalpy, temperature, and specific entropy at the dead state are denoted by h_0, T_0, and s_0, respectively. Following this, the specific chemical exergy is calculated using the equation shown below [21]:

$$\mathrm{ex}_{\mathrm{ch}} = \sum y_i \, \mathrm{ex}_i^{\mathrm{ch},0} + RT_0 \sum y_i \ln y_i \tag{4}$$

The executed analysis determined the mechanism's performance capabilities when functioning within its typical parameters. The essential structure underpinning its operation is clarified by referencing the accompanying chart (Table 1), which exhaustively outlines all the input parameters fed into the synthetic testing environment.

Table 1. Thermodynamic operating parameters of the system [22–24]

parameter	value
Geothermal fluid mass flow rate (kg/s)	1.2
Geothermal production well pressure (kPa)	100
Geothermal production well temperature (°C)	162
Geothermal reinjection well temperature (°C)	69
Geothermal reinjection well pressure (kPa)	30
Isentropic efficiency of turbine (%)	80
Isentropic efficiency of compressor (%)	80
Isentropic efficiency of pump (%)	85
mass flow rate of turbine 1 (kg/s)	14.1
Inlet temperature of PEM electrolyzer (°C)	80
Inlet pressure of PEM electrolyzer (kPa)	100

The absorption heat transformer's coefficient of performance is displayed as follows:

$$\mathrm{COP} = \frac{\dot{Q}_{\mathrm{evaporator}}}{\dot{Q}_{\mathrm{generator}} + \dot{W}_{\mathrm{pump2}}} \tag{5}$$

The formula enables the determination of the modified Rankine cycle production power value:

$$\dot{W}_{\mathrm{ORC}} = \dot{W}_{\mathrm{turb1}} + \dot{W}_{\mathrm{turb2}} - \dot{W}_{\mathrm{pump1}} \tag{6}$$

Water splitting for hydrogen production involves electrolysis, separating hydrogen and oxygen from water. The process starts by heating water in an electrolyzer, transforming a portion into gases. Unreacted water is expelled with oxygen, isolated, and returned to the inlet, yielding final outputs of hydrogen and oxygen. The equations that govern the operation of PEM electrolysis are detailed in Table 2, with the coefficients a, b, and c defined as 3.382, 0.97, and 5.928, respectively.

Table 2. Relationships used for electrolyzer modeling [25, 26]

parameter	Value
PEM electrolyzer work	$W_{\mathrm{PEM}} = 0.25 \times W_{\mathrm{total}}$
Amount of hydrogen produced	$M_{\mathrm{H_2,out}} = a_{\mathrm{H_2}} \times W_{\mathrm{PEM}}^{b_{\mathrm{H_2}}} + c_{\mathrm{H_2}}$
Hydrogen production rate per hour	$N_{\mathrm{H_2,out}} = 3600 \times M_{\mathrm{H_2,out}}$
Theoretical energy for hydrogen production	$\Delta G = \Delta H + T\Delta S$
Electrical energy required	$E_{\mathrm{elec}} = JV$
Electrolytic voltage	$V = V_0 + V_{\mathrm{ohm}} + V_{\mathrm{act},a} + V_{\mathrm{act},c}$
Nernst voltage	$V_0 = 1.229 - 8.5 \times 10^{-4}(T_{\mathrm{PEM}} - 298)$
Anode and cathode overpotential	$V_{\mathrm{act},i} = \frac{RT}{F} \sinh^{-1}\left(\frac{J}{2J_0}\right)$
Exchange current density	$J_0 = J^{\mathrm{ref}} \exp\left(-\frac{E_{\mathrm{act},i}}{RT}\right)$
Ohmic voltage	$V_{\mathrm{ohm}} = JR_{\mathrm{PEM}}$
Total ohmic resistance	$R_{\mathrm{PEM}} = \int_0^L \frac{dx}{\sigma\lambda(x)}$
Local ionic conductivity	$\sigma\lambda(x) = [0.5139\lambda(x) - 0.326] \exp\left[1268\left(\frac{1}{303} - \frac{1}{T}\right)\right]$

The following relationships are employed to assess the system's energy efficiency and exergy [27]:

$$\eta_{\text{energy}} = \frac{W_{\text{ORC}} + W_{\text{chiler}} - W_{\text{PEM}}}{m_1 h_1 - m_5 h_5} \tag{7}$$

$$\eta_{\text{exergy}} = \frac{W_{\text{ORC}} + W_{\text{chiler}} - W_{\text{PEM}} + E_{\text{cooling}}}{m_1 e_1 - m_5 e_5} \tag{8}$$

Exergy is the maximum useful work a system can achieve while achieving equilibrium with its environment, dependent on ambient characteristics. It unifies thermodynamic laws: the First Law focuses on energy conservation and quantity, while the Second Law addresses energy quality and entropy production. Exergy evaluations inform exergoeconomic assessments, enhancing system efficacy by identifying ways to maximize useful work. Assessing exergy in process streams is crucial for strategic planning and optimization efforts. Irreversibilities quantify a system's functional deficiencies, guiding exergy investigations to identify inefficiency locations and causative factors. This process involves two stages: assessing thermodynamic performance gaps via exergy destruction quantification, and identifying optimization opportunities by distinguishing between reducible and inherent exergy losses. Inherent losses are unavoidable due to limitations, while reducible losses indicate potential performance improvements. Exergy analysis reveals inefficiency sources and potential pathways to enhance system design or operation, with Table 3 providing mathematical representations of exergy degradation in a combined heat and power (CHP) system.

Table 3. Exergy destruction relations of different components of the system

component	exergy destruction equation
Absorption cooling cycle absorber	$\dot{\text{E}}\text{x}_{18} + \dot{\text{E}}\text{x}_{24} - \dot{\text{E}}\text{x}_{19} - \text{Ex}_{Q,\text{abs}}$
Absorption cooling cycle generator	$\dot{\text{E}}\text{x}_{21} - \dot{\text{E}}\text{x}_{15} - \dot{\text{E}}\text{x}_{22} + \text{Ex}_{Q,\text{gen}}$
Absorption cooling cycle condenser	$\dot{\text{E}}\text{x}_{15} - \dot{\text{E}}\text{x}_{16} - \text{Ex}_{Q,\text{cond}}$
Absorption cooling cycle evaporator	$\dot{\text{E}}\text{x}_{17} - \dot{\text{E}}\text{x}_{18} + \text{Ex}_{Q,\text{evap}}$
Absorption cooling cycle vapor heat exchanger	$\dot{\text{E}}\text{x}_{20} + \dot{\text{E}}\text{x}_{22} - \dot{\text{E}}\text{x}_{23} - \dot{\text{E}}\text{x}_{21}$
PEM preheater	$\dot{\text{E}}\text{x}_{7} - \dot{\text{E}}\text{x}_{8}$
Rankine cycle pump	$\dot{\text{E}}\text{x}_{12} - \dot{\text{E}}\text{x}_{13} + W_{\text{pump,ORC}}$
Rankine cycle turbine1	$\dot{\text{E}}\text{x}_{6} - \dot{\text{E}}\text{x}_{7} - W_{\text{turb1,ORC}}$
Rankine cycle condenser	$\dot{\text{E}}\text{x}_{11} - \dot{\text{E}}\text{x}_{12}$
Rankine cycle turbine2	$\dot{\text{E}}\text{x}_{9} - \dot{\text{E}}\text{x}_{1}0 - W_{\text{turb2,ORC}}$
PEM Electrolyzer	$\dot{\text{E}}\text{x}_{26} - \dot{\text{E}}\text{x}_{27} - \dot{\text{E}}\text{x}_{28} + W_{\text{Electroliz,PEM}}$
heat exchanger 1	$\dot{\text{E}}\text{x}_{25} + \dot{\text{E}}\text{x}_{4} - \dot{\text{E}}\text{x}_{5} - \dot{\text{E}}\text{x}_{26}$
heat exchanger 2	$\dot{\text{E}}\text{x}_{13} + \dot{\text{E}}\text{x}_{10} - \dot{\text{E}}\text{x}_{14} - \dot{\text{E}}\text{x}_{11}$
Heat recovery vapor generator	$\dot{\text{E}}\text{x}_{3} + \dot{\text{E}}\text{x}_{14} - \dot{\text{E}}\text{x}_{9} - \dot{\text{E}}\text{x}_{4}$
Claude cycle compressor	$W_{\text{comp,rev}} - W_{\text{comp,act}}$
Claude cycle heat exchanger 1	$\dot{\text{E}}\text{x}_{31} + \dot{\text{E}}\text{x}_{40} - \dot{\text{E}}\text{x}_{41} - \dot{\text{E}}\text{x}_{32}$
Claude cycle heat exchanger 2	$\dot{\text{E}}\text{x}_{32} + \dot{\text{E}}\text{x}_{42} - \dot{\text{E}}\text{x}_{33} - \dot{\text{E}}\text{x}_{43}$
Claude cycle heat exchanger 3	$\dot{\text{E}}\text{x}_{33} + \dot{\text{E}}\text{x}_{39} - \dot{\text{E}}\text{x}_{34} - \dot{\text{E}}\text{x}_{40}$
Claude cycle heat exchanger 4	$\dot{\text{E}}\text{x}_{34} + \dot{\text{E}}\text{x}_{44} - \dot{\text{E}}\text{x}_{45} - \dot{\text{E}}\text{x}_{35}$
Claude cycle heat exchanger 5	$\dot{\text{E}}\text{x}_{35} + \dot{\text{E}}\text{x}_{38} - \dot{\text{E}}\text{x}_{36} - \dot{\text{E}}\text{x}_{39}$

4 Economic Analysis

Optimizing thermal engineering infrastructure requires a holistic framework that integrates first-law and second-law analyses with fiscal assessment. Thermoeconomics bridges energy quality and financial metrics by combining exergy analysis with monetary evaluation, aiming to reduce operational costs through optimal energy resource management. This methodology offers analytical advantages beyond traditional models by using exergy as the basis for monetizing thermodynamic degradation. Key steps include exergy assessment, financial analysis, exergy-based pricing, and predictive thermoeconomic metrics formulation. The research identifies optimal operational parameters by aligning thermodynamics with financial data, analyzing energy flow, exergy utilization, and economic impact, resulting in accurate cost per functional output unit for the entire system. The following equation represents the steady-state economic equilibrium for system costs:

$$\dot{C}_{P,\text{total}} = \dot{C}_{F,\text{total}} + \dot{Z}_{CI,\text{total}} + \dot{Z}_{\text{OM,total}} \tag{9}$$

The application of a thermoeconomic framework offers significant utility for the comprehensive evaluation of

energy systems. Building on this advantage, our investigation proceeds to compute the facility's levelized cost of energy (LCOE) and hydrogen (LCOH), utilizing the subsequent criteria [28]:

$$\mathrm{LOCE} = \frac{\mathrm{AOC}}{(W_{\mathrm{total}} + Q_{\mathrm{cooling}} + Q_{\mathrm{heating}}) \times \tau} \tag{10}$$

$$\mathrm{LCOH} = \frac{\mathrm{AOC}}{(\mathrm{LHV}_{\mathrm{H_2}} \dot{N}_{\mathrm{H_2}} \dot{m}_{\mathrm{H_2}} + Q_{\mathrm{cooling}} + Q_{\mathrm{heating}}) \times \tau} \tag{11}$$

The system's annual operating hours (τ) are assumed to be 8,000 per year. The Annual Operating Cost (AOC) is determined as follows:

$$\mathrm{AOC} = \mathrm{TOC} \times \phi \times \mathrm{CRF} \tag{12}$$

The term TOC (Total Operating Costs) encompasses the aggregate sum of all running expenditures. A maintenance augmentation factor, symbolized by ϕ, is stipulated at a value of 1.06, adhering to the precedent set in reference [29]. The variables i and n correspond, respectively, to the prevailing rate of interest and the power station's projected duration of active service. Based on these inputs, the Capital Recovery Factor (CRF) is consequently derived as [30]:

$$\mathrm{CRF} = \frac{i(1+i)^n}{(1+i)^n - 1} \tag{13}$$

To precisely determine the expense rate of a system, economic considerations including interest rates and the capital recovery factor are employed. This resultant yearly expense is subsequently divided by 7,446 operational hours to ascertain the system's cost per hour [31].

$$Z_{\mathrm{total}} = \frac{\mathrm{TOC} \times \phi \times \mathrm{CRF}}{t} \tag{14}$$

Within this framework, 'n' signifies the operational duration, and 'i' corresponds to the prevailing interest rate. Table 4 elucidates the pivotal interdependencies leveraged to harmonize energy output with financial expenditure factors. Achieving congruence between these crucial parameters establishes the economic practicality of meeting power generation targets concurrently with stringent expenditure management. The judicious application of these linkages consequently elevates the comprehensive operational efficacy of the system while ensuring peak fiscal optimization.

Table 4. Cost functions of different components of the system [32, 33]

component	cost function
Absorption cooling cycle generator	$z = 17500 \times \left(\frac{A_{\mathrm{gen}}}{100}\right)^{0.6}$
Absorption cooling cycle condenser	$z = 8000 \times \left(\frac{A_{\mathrm{cond}}}{100}\right)^{0.6}$
Absorption cooling cycle absorber	$z = 16000 \times \left(\frac{A_{\mathrm{abs}}}{100}\right)^{0.6}$
Absorption cooling cycle evaporator	$z = 16000 \times \left(\frac{A_{\mathrm{evap}}}{100}\right)^{0.6}$
Absorption cooling cycle steam heat exchanger	$z = 12000 \times \left(\frac{A_{\mathrm{SHE}}}{100}\right)^{0.6}$
Organic Rankine Cycle Condenser	$z = 516.62 \times (A_{\mathrm{cond}})^{0.6}$
Organic Rankine Cycle Turbine	$z = 4750 \times W_{\mathrm{turb}})^{0.75}$
organic Rankine cycle pump	$z = 200 \times (W_{\mathrm{pump}})^{0.65}$
organic Rankine cycle heat exchanger1	$z = 130 \times \left(\frac{A_{\mathrm{heat\ exchanger}}}{0.093}\right)^{0.78}$
organic Rankine cycle heat exchanger 2	$z = 4122 \times (A_{\mathrm{heat\ exchanger}})^{0.6}$
organic Rankine cycle compressor	$z = 7900 \times (W_{\mathrm{comp}})^{0.62}$
Claude cycle heat exchanger	$z = 8500 + 409 \times (A_{\mathrm{heat\ exchanger}})^{0.8}$
PEM electrolyzer cycle	$Z = 1000 \times W_{\mathrm{elec}}$

5 Genetic Algorithm Optimization of the System

Inspired by the adaptive mechanisms found in biological life, a genetic algorithm functions as an optimization technique. This computational approach is specifically classified as a numerical, direct, and probabilistic search methodology. Operating in an iterative fashion, it draws upon principles from genetic science, mimicking natural evolutionary processes to effectively leverage the knowledge embedded within a given population for the purpose of generating novel and enhanced solutions. As optimization algorithms operating within a computational framework, Genetic Algorithms excel at intelligently sifting through various segments of the solution spectrum. They achieve this by appraising multiple candidate solutions concurrently in each generation, and notably, their search process avoids the computationally intensive task of defining the objective function across the entirety of the solution set. Instead, the objective function's computed value at each data point feeds into a statistical aggregation process. This process reveals the objective function's behavior across relevant sub-regions. These sub-regions are then processed concurrently through parallel statistical averaging, leveraging their individual objective function data. This inherent parallel processing, termed implicit parallelism, guides the search towards regions of higher average objective function values, thus improving the chances of discovering a global optimum.

In contrast to conventional optimization methods that may become confined to narrow search trajectories, this algorithm's continuous and extensive interrogation of the entire domain substantially diminishes the risk of premature convergence to a suboptimal finding. A notable advantage stemming from this design is its independence from functional regularity; specifically, the algorithm imposes no prerequisites regarding mathematical traits such as differentiability or requisite smoothness. This optimization method functions by exclusively assessing the objective function at various input values, completely disregarding any derivative information or other supplementary data. To achieve a favorable trade-off between enhanced precision in finding optimal solutions and reduced computational effort, the simulation employed a population of 100 individuals and ran for a maximum of 200 generations. During the optimization, a crossover rate of 0.8 was utilized, and the mutation rate was established at 0.05. The optimization parameters in a genetic algorithm have the following defined ranges: the compressor compression ratio varies between 180 and 220, the turbine isentropic efficiency ranges from 65% to 85%, and the compressor isentropic efficiency falls between 72% and 92%.

6 Validation

This investigation unveils a groundbreaking system architecture designed for parallel manufacturing operations. Its operational efficacy undergoes rigorous validation through a comparative analysis, juxtaposing its performance against empirical data compiled in Table 5 and the established findings of Arora et al. [34].

Table 5. Validation of the proposed system utilized Arora et al.'s evaluation [34]

Parameter	obtained results	Reference results
absorbent heat (kW)	2943	2945.26
condenser heat (kW)	2506	2505.91
evaporator heat (kW)	2355	2355.4
coefficient of performance	0.79	0.7609
absorptive exergy destruction (kW)	70.16	70.478
condenser exergy destruction (kW)	6.606	6.066
evaporator exergy destruction (kW)	86.28	86.275

For the purpose of this analysis, the system model is configured under ambient conditions of 25 °C and a pressure of 101 kPa. Fundamental modeling postulates include the assumption that both temperature and pressure remain effectively constant as process fluids circulate through the system's various constituent components. Furthermore, it is posited that the solutions exiting the absorber and generator stages achieve saturation, aligning with their respective equilibrium temperatures and solute concentrations. The system postulates that the vapor exiting the evaporator and the refrigerant within the condenser both exist in a saturated state, each corresponding to its specific saturation temperature. Furthermore, the superheated refrigerant vapor that emerges from the generator is assumed to be at the generator's operating temperature.

The study accounts for realistic operational scenarios, incorporating non-equilibrium conditions at the ingress points of both the generator and the absorber, as well as considering the state of fluids leaving the solution pump and the heat exchanger. To support a refrigerant mass flow of 1 kg/s, the generator and its associated heat source are maintained at a uniform temperature ranging from 87 to 88 °C. With the condenser and absorber concurrently operating at 37.8 °C, and the evaporator holding steady at 7.2 °C, the comparative analysis yielded remarkably similar outcomes. The minimal discrepancies observed unequivocally attest to the high precision of the validation method.

7 Environmental Analysis

The evaluation and execution of energy systems significantly depend on the necessity of performing environmental analyses. This practice promotes a comprehensive understanding of the potential ecological impacts associated with energy production, distribution, and consumption. The range of such studies goes beyond traditional energy assessments, considering various elements such as carbon emissions, habitat destruction, and resource depletion. By incorporating environmental factors into the decision-making process, stakeholders can successfully identify and alleviate possible negative effects while fostering sustainability practices and resource conservation. As a result, the integration of environmental analysis facilitates the development and management of energy systems in a way that reduces their ecological footprint and supports a sustainable and resilient future.

8 Results and Discussion

Thermodynamics has traditionally been defined by its focus on energy and entropy, as dictated by its first and second laws. A fresh understanding, however, presents thermodynamics as the science of energy and exergy, a framework that more seamlessly integrates both laws. This perspective enables ongoing measurement of energy and exergy within a system, thereby permitting the calculation of vital efficiencies via thorough energy and exergy analysis. The true value of a system's operational effectiveness is best gauged by its exergy efficiency, as this metric provides the most accurate and precise assessment of performance. Leveraging both energy and exergy accounting has become a globally accepted thermodynamic methodology for the evaluation and comparison of industrial processes and mechanical configurations. This framework is robustly grounded in the fundamental theorems established by the First and Second Laws of Thermodynamics. Because of its comprehensive nature, this analytical approach is widely recognized as the most logical and insight-driven procedure available for systematically benchmarking disparate systems against one another. Building upon the computational framework previously outlined, we meticulously determined crucial thermodynamic state variables, including thermal energy, pressure potential, specific heat content, and disorder, for all points throughout the studied system. Thereafter, the fundamental principle of energy conservation, as described by the First Law of Thermodynamics, was applied and solved for each constituent element of the cycle. The exergy evaluation commenced by employing the two specified formulae to quantify the aggregate exergy associated with each constituent part. This foundational calculation subsequently enabled the determination of the latent exergy content, the projected exergy expenditures, and the overall exergy conversion efficiencies pertaining to the complete operational loop. This estimation methodology proved crucial for singling out the system's elements that exhibited the most substantial exergy values, and for subsequently appraising their individual operational effectiveness. Table 6 comprehensively illustrates the outcomes derived from the thermodynamic assessment of the conceptualized system.

Table 6. Results of thermodynamic evaluation

parameter	value
system energy efficiency (%)	45
system exergy efficiency (%)	53
hydrogen production rate(kg/h)	4.88
Output power of PEM electrolyzer cycle(kw)	475.1
Output power of liquefaction cycle(kw)	13.77
Total output power(kw)	1425

The exhaustive thermodynamic assessment conducted on the deep-earth thermal resource employed water as the principal operational medium. This rigorous evaluation established a mechanical output capability of 1,425 kilowatts. Furthermore, the analysis determined the thermal effectiveness (energy efficiency) to be 45%. The corresponding quality factor (exergy efficiency) was found to be slightly superior, registering 53%. A foundational principle governing all genuine operational cycles is the consistent consumption of available work potential, meaning the incoming exergy invariably exceeds the outgoing exergy. This inevitable deficit stems entirely from inherent process imperfections and is scientifically labeled as exergy destruction. It is essential to precisely delineate the internal dissipation of exergy, which inherently arises from thermodynamic imperfections, from the external efflux of exergy, representing valuable, unutilized energy discharged into the surroundings. While both these

phenomena underscore a decline in energy quality, the concept of irreversibility itself lacks the direct exergy-specific or environmental framing that characterizes exergy loss. Analysis of the system revealed substantial thermodynamic losses, evident as significant exergy destruction, primarily concentrated in the Proton Exchange Membrane (PEM) electrolyzer and the Organic Rankine Cycle (ORC) components, specifically the turbine and condenser. In contrast, the pumps exhibited the lowest levels of exergy dissipation among all system elements. The total exergy loss across the entire system was quantified at 56,140 kW. A detailed breakdown of exergy destruction for each individual component is presented in Table 7.

Table 7. Exergy destruction results of different components of the system

parameter	value
PEM electrolyzer (kw)	47295
evaporator of the absorption cooling cycle (kw)	86.29
ORC Cycle Pump (kw)	2.196
ORC cycle turbine 1 (kw)	1255
ORC cycle turbine 2 (kw)	1849
condenser of absorption cooling cycle (kw)	6.62
PEM Preheater (kw)	2831
ORC Cycle Condenser (kw)	252
absorption cooling cycle generator (kw)	49.96
expansion valve of the absorption cooling cycle (kw)	6.934
vapor heat exchanger absorption cooling cycle (kw)	6.33
heat exchanger 1 (kw)	5.094
heat exchanger 2 (kw)	6.328
heat recovery vapor generator (kw)	840.5
Claude cycle Compressor (kw)	7.277
Claude cycle heat exchanger 1 (kw)	81.16
Claude cycle heat exchanger 2 (kw)	14.07
Claude cycle heat exchanger 3 (kw)	79.67
Claude cycle heat exchanger 4 (kw)	6.328
Claude cycle heat exchanger 5 (kw)	117.4

The financial advantages are determined through an examination of how businesses can strategically incorporate co-products into their operations, aiming to either amplify income streams or diminish waste management expenditures. This evaluation covers tangible advantages, such as decreased input material and transportation expenses, alongside intangible benefits like an enhanced reputation and more straightforward regulatory approvals. Following this, a thorough economic feasibility study of the suggested system is undertaken. This analysis integrates updated cost algorithms for each element, ensuring optimal operational efficiency across a wide spectrum of applications. The specific cost rates for the system's constituent parts are itemized within Table 8.

Table 8. Results of cost rates of different components of the system

parameter	value
Absorption cooling cycle absorber ($/h)	31992
ORC cycle pump ($/h)	1178
ORC cycle turbine 1 ($/h)	403275
Absorption cooling cycle condenser ($/h)	11291
absorption cooling cycle generator ($/h)	17484
vapor heat exchanger absorption cooling cycle ($/h)	9322
ORC cycle turbine 2 ($/h)	1185755
PEM preheater ($/h)	21213
PEM electrolyzer ($/h)	5038654
ORC cycle condenser ($/h)	8698
absorption cooling cycle evaporator ($/h)	36134
Claude cycle Compressor ($/h)	40152
Claude cycle heat exchanger 1 ($/h)	8544
Claude cycle heat exchanger 2 ($/h)	8549
Claude cycle heat exchanger 3 ($/h)	8520
Claude cycle heat exchanger 4 ($/h)	8516
Claude cycle heat exchanger 5 ($/h)	8609

The sustained triumph of this system is fundamentally contingent upon its financial viability. By fostering synergistic partnerships with adjacent industrial entities, enterprises can effectively curtail logistical expenditures, diminish waste management outlays, and monetize valuable co-products. To thoroughly assess the proposed system's economic feasibility, an exergoeconomic investigation was also undertaken, which pinpointed an overarching hourly expense rate of $37.16 for the specific scenario examined. Supplementary core findings from this financial appraisal are presented in Table 9. Two paramount indicators in the system's economic evaluation are the levelized cost of hydrogen production (LCOH) and the levelized cost of electricity generation (LCOE), which were determined to be $24.39 per kilogram and 19.8 cents per kilowatt-hour, respectively.

Table 9. Results of economic analysis

parameter	value
LCOE (cent/kWh)	19.8
LCOH ($/kg)	24.39
CRF	18
Total cost of system ($/h)	37.16

The efficiency and cost rate of the proposed system were compared with other systems and, as shown in Table 10, the studied system has the appropriate implementation capability and effectiveness in various industrial applications.

Table 10. Results of economic analysis

parameter	Present work	Alirahimi et al. [35]	Emadi et al. [36]
Exergy efficiency (%)	53	21.63	24.92
Total cost ($/h)	37.16	63.89	423.5

8.1 Conduction of sensitivity analysis

An analysis of how system design parameters influence performance is presented in this section. Specifically, the study analyzes the influence of thermodynamic factors like turbine efficiency, outlet temperature and pressure of turbine 1, and outlet temperature of thermal recovery steam generator on system performance criteria.

8.1.1 Effect of the variation of the isentropic efficiency of turbine

As demonstrated in Figure 2, changes in turbine efficiency profoundly influence several critical system attributes. These include the quantity of power produced, the cumulative exergy loss, the associated economic cost, and the overall energetic and exergetic efficiencies. A clear trend is evident: an improvement in turbine efficiency, specifically from 75% to 85%, directly leads to a higher net power generation. This enhanced output directly results from the turbine's improved capability to convert energy into useful work, a function fundamental to electricity production. An uptick in power generation directly benefits the electrolyzer's functionality, fostering a higher rate of hydrogen synthesis within the system. Concurrently, optimizing turbine efficiency translates into elevated energy and exergy efficiencies, alongside noteworthy economic advantages. This positive correlation between generated power and exergy efficiency is distinctly illustrated in the accompanying diagram. Overall, the system has demonstrated enhanced operational effectiveness, evidenced by its increased capacity for energy and work production. Nonetheless, this advancement has been met with escalating expenditures. These higher financial burdens stem from not only the increased investment in equipment and production processes but also from the indirect costs associated with system downtimes and interruptions. A key financial drawback has been the suboptimal economic return on our production capacity. This inefficiency has directly inflated comprehensive system costs, as every individual component contributes its own fiscal burden. Thermodynamically speaking, exergy represents the practical work extracted from the turbine, with energy conversion effectiveness directly mirroring the aggregate work produced. Consequently, optimizing turbine performance is critical. This will fundamentally enhance the system's thermal dynamics, resulting in elevated gross energy and available exergy levels, a boost in net power output, and a significant curtailment of energy degradation.

8.1.2 Effect of the variation of the pressure at the outlet of the turbine 1

Figure 3 comprehensively illustrates the system's response to fluctuations in Turbine 1's discharge pressure, specifically detailing its influence on net power generation, irreversibility (exergy destruction), operational cost, and the overall energy and exergy efficiencies. A clear trend emerges, indicating that an escalation in this exit pressure consistently correlates with an intensified rate of exergy destruction. This situation inevitably leads to elevated energy dissipation along with a degradation in the system's overall operational effectiveness. Furthermore, a decline in both energy and exergy conversion efficiencies is consistently observed, a consequence of their intrinsic connection to the power generated and the system's exergy state. By contrast, deliberately scaling back the system's power output mitigates the necessity for expensive, high-performance thermodynamic components. This strategy, therefore, results in a reduced levelized cost for electricity generation, hydrogen synthesis, and the total system expenditure.

8.1.3 Effect of the variation of the temperature at the outlet of the turbine 1

Figure 4 visually articulates how the exhaust temperature of Turbine 1 modulates the system's energy and exergy utilization effectiveness, its operational cost implications, the rate of power generation, and the extent of exergy irreversibility. Within the thermal window spanning 70 to 90 °C, an escalation in temperature demonstrably intensifies internal system inefficiencies and exergy destruction. This, in turn, leads to a significant decline in the generated power output and detrimentally impacts both the energetic and exergetic performance of the system. Surprisingly, a more modest production output can actually bolster financial sustainability. This is achieved through a reduction in the long-term, per-unit cost of both hydrogen and electricity, alongside a decrease in the ongoing capital investment associated with larger-scale equipment.

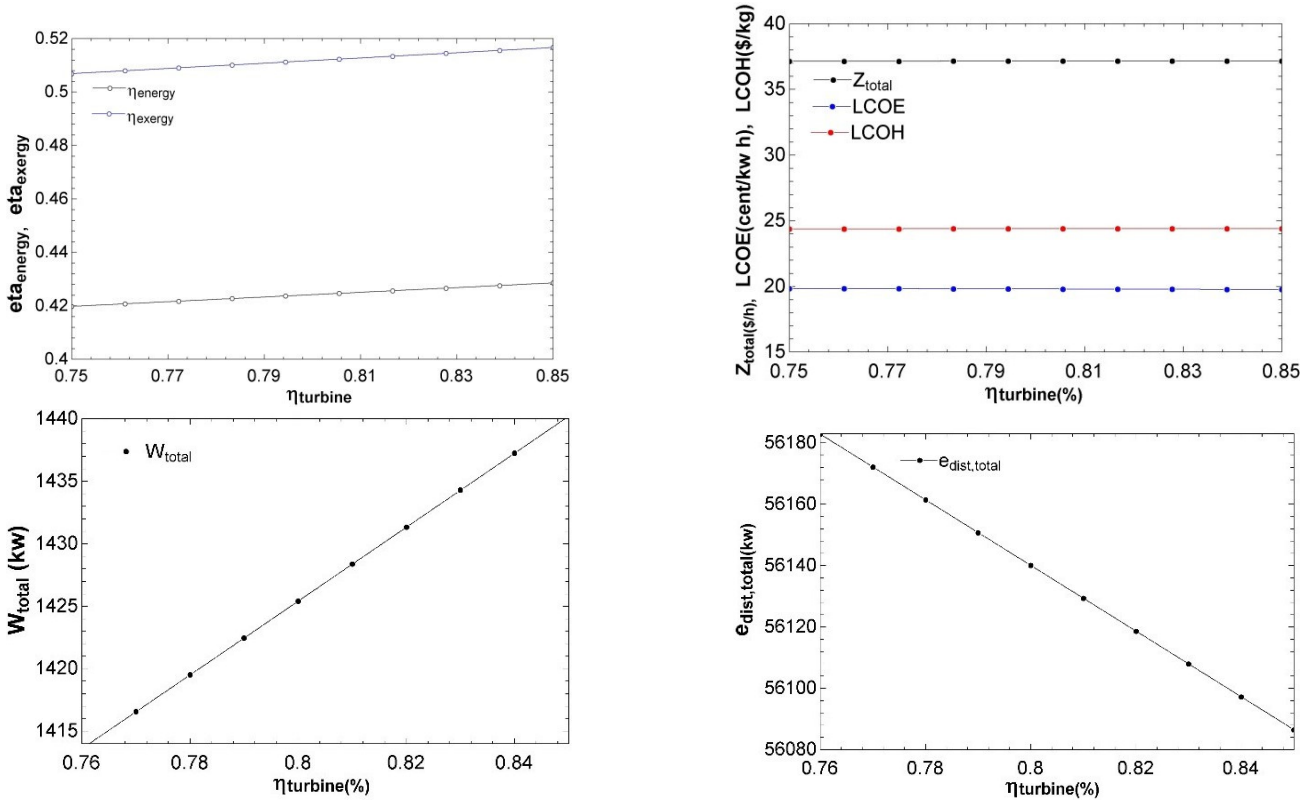

Fig. 2. Effect of the variation of the isentropic efficiency of turbine

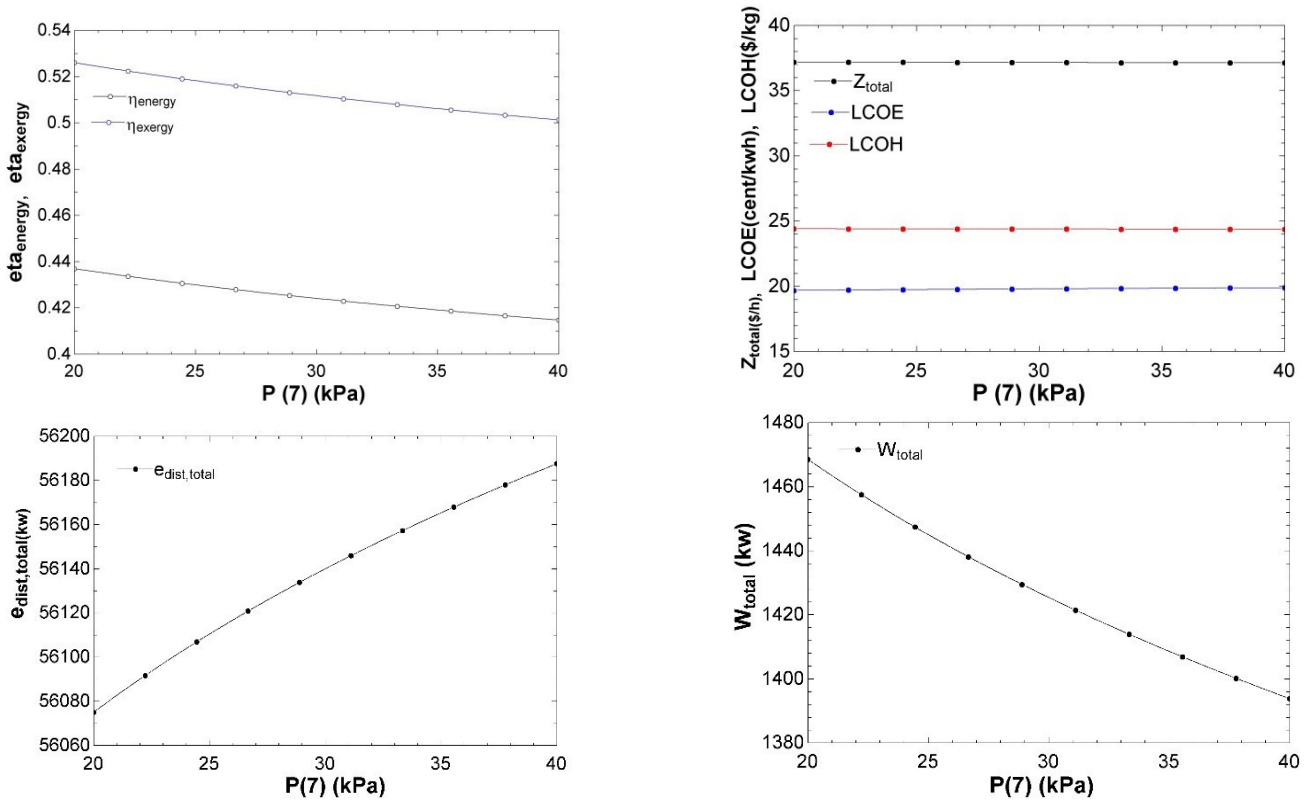

Fig. 3. Effect of the variation of the pressure at the outlet of the turbine 1

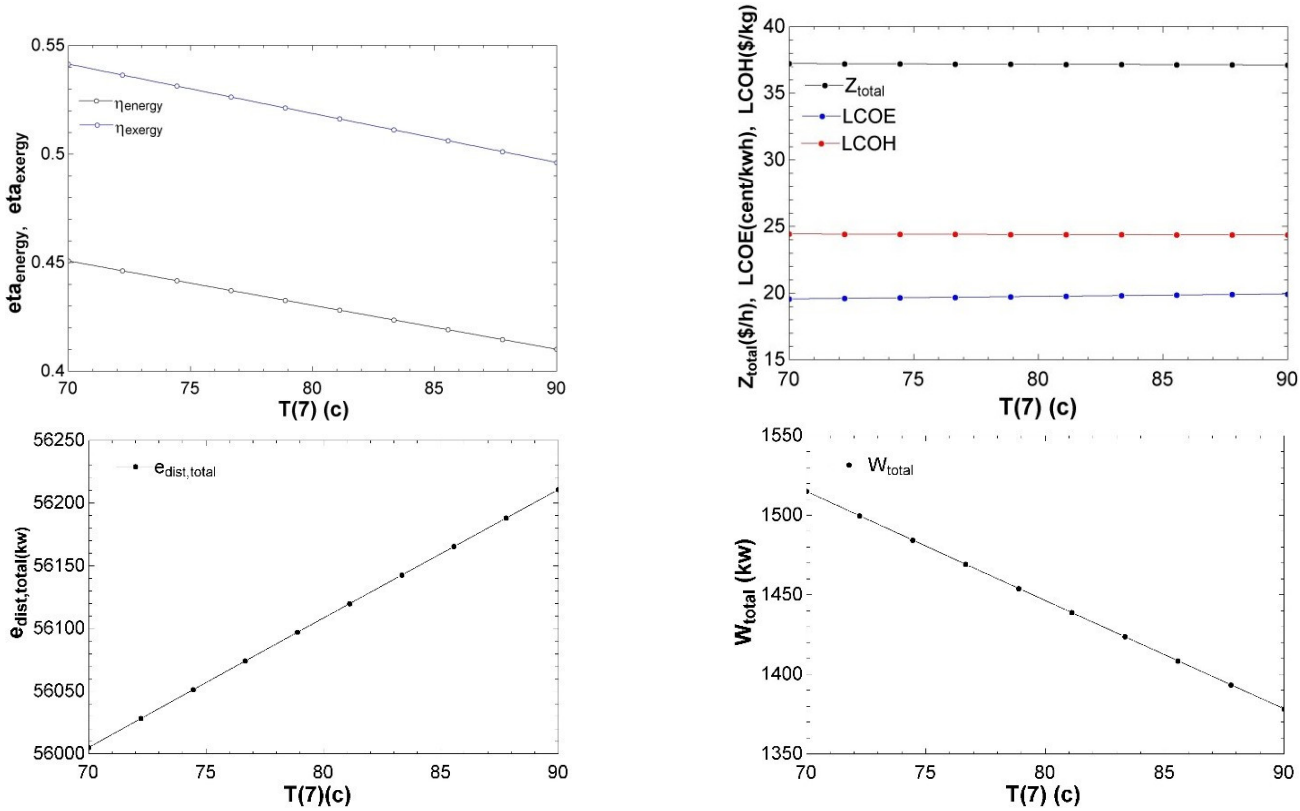

Fig. 4. Effect of the variation of the temperature at the outlet of the turbine 1

8.1.4 Effect of the variation of the temperature at the outlet of the thermal recovery steam generator

The influence of the heat recovery steam generator's (HRSG) terminal temperature on the modified Rankine cycle's power output, exergy destruction, cost rate, and overall energy and exergy efficiencies is investigated in Figure 5. Critically, a greater HRSG outlet temperature translates to a diminished heat transfer to the ORC working fluid, consequently lowering its thermal energy input. Achieving a more conservative use of energy, while reducing overall thermodynamic losses, concurrently curtails the electrical yield of the ORC turbine. A reduction in the cycle's operational inlet temperature impairs the system's thermal energy uptake, consequently weakening its capacity for electricity generation. This subsequent shortfall in power constrains the turbine, lessening the electrical supply it can provide to the electrolyzer and thereby hindering the rate of hydrogen synthesis. Furthermore, given the fundamental relationship between a system's output capacity, its exergy performance, and the associated unit costs, any reduction in power generation will inevitably result in diminished thermodynamic efficiency and increased production expenses for both hydrogen and electricity.

8.2 Two objective optimization

The pursuit of ideal operational outcomes for objective functions and critical structural variables within sprawling, sophisticated architectures constitutes an immense modeling difficulty. This significant degree of intricacy often stems from the intrinsic attributes of the performance metrics themselves, the sheer volumetric scale of adjustable factors, and the pervasive influence of underlying nonlinear foundational equations. Fortunately, Genetic Algorithms (GAs) furnish a resilient and powerful computational approach designed to reliably pinpoint optimal remedies within these highly constrained and convoluted environments, doing so by directly harnessing the core mechanisms of Darwinian natural selection. This investigation employed a dual-objective genetic algorithm to identify the most favorable operating conditions and performance metrics for the proposed system. The central aim was to enhance the system's thermodynamic performance by simultaneously minimizing operational expenses while maximizing both energy and exergy efficiencies. Through this optimization, the ideal values for the design variables and their corresponding objective functions were

precisely determined. The optimal configuration, detailed in Table 11, reveals that the system can achieve an energy efficiency of 46%, an exergy efficiency of 54%, and an hourly operating cost of $37.07 when functioning under these peak conditions.

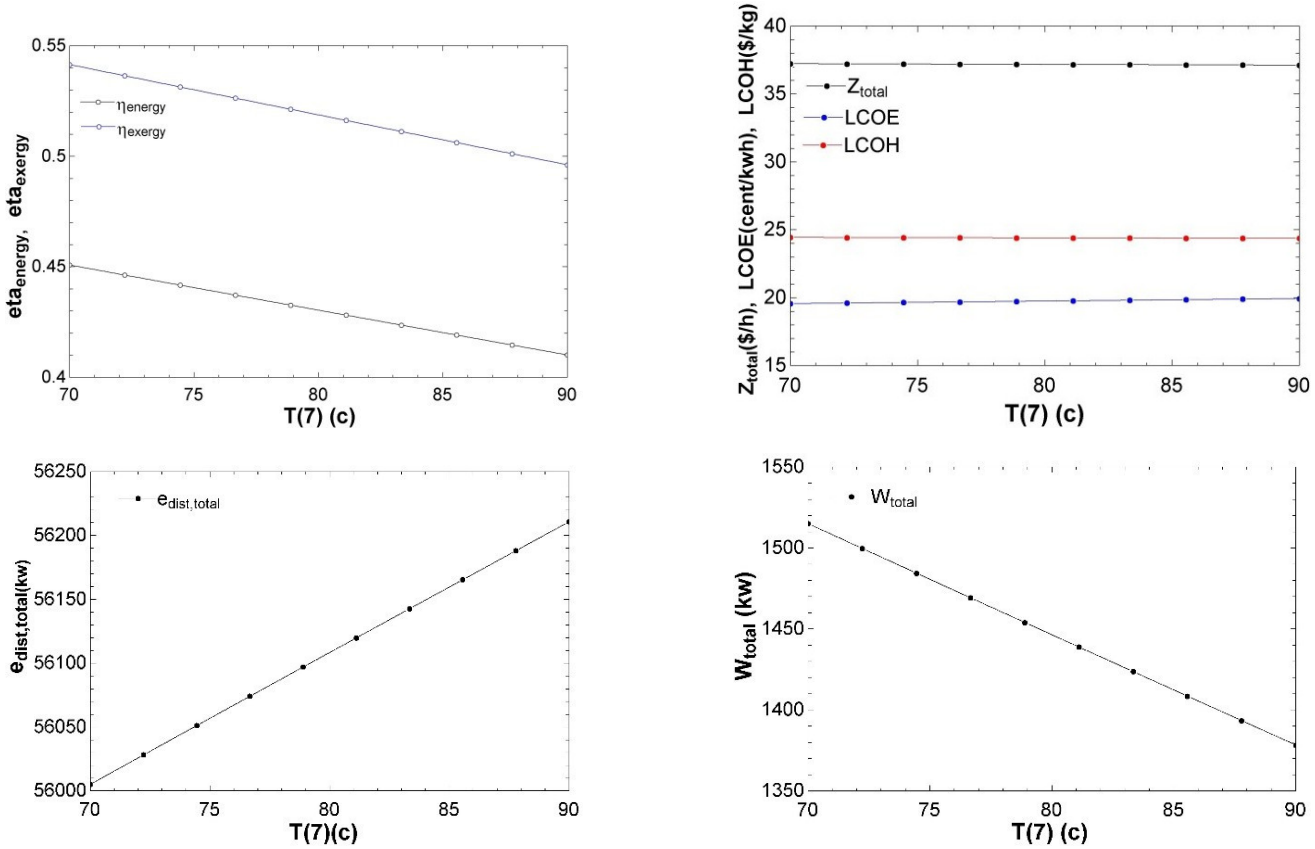

Fig. 5. Effect of the variation of the temperature at the outlet of the thermal recovery steam generator

Table 11. Optimal values

Decision variable	Optimum case
total cost of system($/h)	37.07
exergy efficiency of system (%)	54
energy efficiency of system (%)	46
Isentropic efficiency of turbine (%)	70
Isentropic efficiency of compressor (%)	87
Isentropic efficiency of pump (%)	82
Outlet pressure of turbine 1 (kPa)	49.95
inlet temperature of turbine 2 (°C)	133.3
LCOE (cent/kWh)	19.62
LCOH ($/kg)	24.41

Envisioned with ecological longevity at its core, this geothermal installation harnesses inexhaustible energy sources, delivering clean power while significantly mitigating its ecological footprint. The performance enhancement methodology employed a Pareto efficiency frontier, mapping optimal trade-offs across three distinct operational contexts. Subsequently, the Technique for Order of Preference by Similarity to Ideal Solution (TOPSIS) was utilized to rigorously appraise candidate solutions and pinpoint the most efficacious operational setting. A profound comprehension of the dynamic relationship between expenditure levels and operational throughput is indispensable for discerning the inherent compromises between these critical objectives. This section, illustrated in Figures 6, 7, and 8, details the performance outcomes of the system's optimization across various scenarios. Specifically, Figure 6 highlights the ideal operating point (indicated in red) determined by the TOPSIS methodology, taking into account both exergy efficiency and the overall cost of operation. Moving on, Figure 7 illustrates the interplay between energy efficiency and the averaged cost of generating electricity. Finally, Figure 8 explores the connection between energy efficiency and the averaged cost of producing hydrogen.

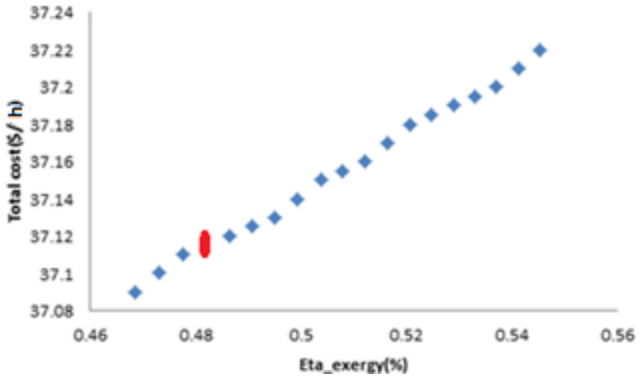

Fig. 6. Pareto diagram considering exergy efficiency and total cost

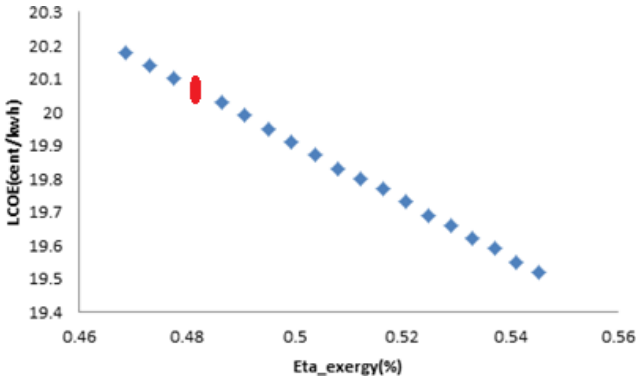

Fig. 7. Pareto diagram considering exergy efficiency and levelized cost of electricity generation

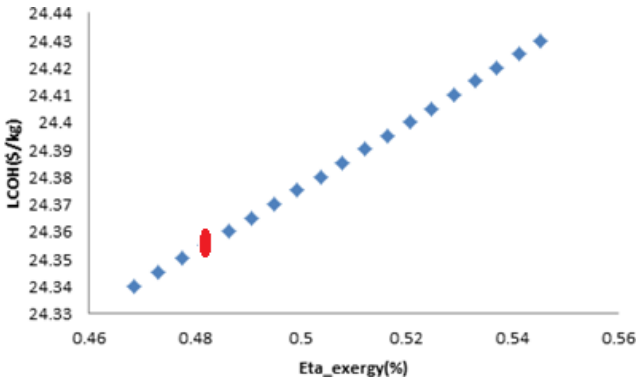

Fig. 8. Pareto diagram considering exergy efficiency and levelized cost of hydrogen production

9 Conclusion

A comprehensive evaluation was executed, spanning energy efficiency, exergy accounting, and thermoeconomic viability. This assessment specifically focused on an innovative, integrated configuration composed of a modified Rankine cycle directly coupled with a hydrogen generation unit, all driven solely by geothermal energy. The entire hybrid setup was simulated and its detailed thermodynamic and economic performance analyzed through the application of EES software. An in-depth parametric sensitivity analysis was further carried out on the integrated system to unravel the intricate connections between its operational variables and the defined performance metrics. Heat constitutes an indispensable input for industrial operations, yet these processes habitually discharge considerable quantities of energy as waste during their routine functioning. Propelled by the escalating expenses of manufacturing, numerous initiatives have focused on recuperating this discarded thermal energy. In this investigation, a thorough thermodynamic (energy and exergy) and financial evaluation was performed on a novel poly-generation cycle.

The operational methodology detailed here facilitates the concurrent generation of three distinct utility streams – thermal energy, chilling capacity, and electrical output – through a highly integrated system architecture. This infrastructure is founded upon the synergistic deployment of Organic Rankine Cycle units, a thermally-activated absorption cooling apparatus, a Proton Exchange Membrane (PEM) cell dedicated to electrolysis, and a specialized mechanism for converting the resulting hydrogen gas into its liquid phase. This entire analytical framework is strictly governed by the foundational tenets of the First and Second Laws of Thermodynamics. A simulation of the combined cycle was conducted, adhering to the first and second laws of thermodynamics for its constituent parts. The system offers substantial efficiency gains by minimizing the energy input needed for liquid hydrogen generation. This is accomplished by first pre-cooling the hydrogen with an absorption chiller and subsequently exposing it to two liquid nitrogen bath heat exchangers. The PEM unit represents the primary source of inefficiency, responsible for 84% of the overall energy loss in the integrated multi-generation setup. Conversely, the bulk energy dissipation is apportioned among three components: the Claude circuit, which accounts for 3% of the total exergy destruction; the absorption refrigeration mechanism, which accounts for 1%; and the Organic Rankine Cycle (ORC), which is responsible for the largest share at 12%. Of all components within the integrated plant, the ORC electrolyzer represents the primary locus of thermodynamic irreversibility. This extreme level of destruction can be dramatically curtailed through the straightforward intervention of elevating the input stream temperature, thereby yielding a marked improvement in the system's overall operational efficacy.

Accordingly, this study provides a meticulous investigation into how critical operational parameters dic-

tate the machine's efficiency metrics. The performance of this system was examined by altering four critical factors: the isentropic efficiency of the turbine, the pressure at the turbine's first outlet, the final temperature from the thermal recovery steam generator, and the temperature at the turbine's first outlet. Our parametric analysis showed that a higher isentropic efficiency for the turbine led to enhanced energy generation, improved exergy efficiency, and greater overall power production. Conversely, raising the pressure and temperature downstream of the turbine's initial stage negatively affected the system's power output and lowered its energy efficiency. To pinpoint the ideal settings for operation, we then utilized multi-objective optimization approaches. While the project's foundational effort was initially dedicated to honing the technical parameters and maximizing mechanical efficiency, a comprehensive financial assessment is reserved for a subsequent chapter. This assessment will specifically quantify the lifecycle production costs for both hydrogen and electrical power, thereby allowing for a definitive determination of the system's overall monetary viability.

An in-depth economic analysis has revealed that the electrolyzer component accounts for a significant majority, specifically 73%, of the overall expenses associated with the multi-generation system. The remaining costs are distributed among the absorption refrigeration unit (23%), the hydrogen liquefaction cycle (1%), and the modified Rankine cycle (3%). The internal structure, benefiting from meticulously integrated constituents, yields inherently robust operation and high output metrics, successfully achieving an energetic conversion rate of 45% and an exergetic efficacy of 53%. Financial assessment was instrumental in executing the design process, ensuring the development of a minimally burdensome cost profile. The resulting data established the system's total required running expenditure at just 37.16 $/h, thereby confirming its outstanding monetary viability. By pinpointing the ideal operational sweet spot, multi-objective optimization dramatically cuts a system's expenditure rate and enhances its energy conservation capabilities. Employing evolutionary computation, this approach yields a remarkable 54% boost in energy efficiency, resulting in an aggregate cost rate of 37.07 $/h. Based on the environmental assessment conducted on the system, the carbon dioxide emission rate is calculated to be 0.6 kg/MWh, which indicates the compatibility of the studied system with the environment for the development of sustainable energy systems.

References

[1] Ifaei P, Nazari-Heris M, Charmchi AST, Asadi S, Yoo C. Sustainable energies and machine learning: An organized review of recent applications and challenges. Energy. 2023;266:126432.

[2] Shinde TU, Dalvi VH, Patil RG, Mathpati CS, Panse SV, Joshi JB. Thermal performance analysis of novel receiver for parabolic trough solar collector. Energy. 2022;254:124343.

[3] Dan M, He A, Ren Q, Li W, Huang K, Wang X, et al. Multi-aspect evaluation of a novel double-flash geothermally-powered integrated multigeneration system for generating power, cooling, and liquefied Hydrogen. Energy. 2024;289:129900.

[4] Mahdavi N, Ghaebi H, Minaei A. Proposal and multi-aspect assessment of a novel solar-based trigeneration system; investigation of zeotropic mixture's utilization. Applied Thermal Engineering. 2022;206:118110.

[5] Azizi S, Shakibi H, Shokri A, Chitsaz A, Yari M. Multi-aspect analysis and RSM-based optimization of a novel dual-source electricity and cooling cogeneration system. Applied Energy. 2023;332:120487.

[6] Mahmood Mejbel Ghrairi S, Khalilian M, Mirzaee I. Thermodynamic and thermoeconomic analysis of a multigeneration system using solar and geothermal energies. Hydrogen, Fuel Cell & Energy Storage. 2025;12(1):19-30.

[7] Hai T, Radman S, Abed AM, Shawabkeh A, Abbas SZ, Deifalla A, et al. Exergo-economic and exergo-environmental evaluations and multi-objective optimization of a novel multi-generation plant powered by geothermal energy. Process Safety and Environmental Protection. 2023;172:57-68.

[8] Al-Aayedi ARA, Khalilian M, Chitsaz A, Mirzaee I, Shirvani H. Parametric Study of an ORC-EJR Cycle Based on Energy and Exergy Analysis for Power, Heating, Cooling, and Hydrogen Production. Hydrogen, Fuel Cell & Energy Storage. 2025;12(2):75-82.

[9] Abdollahi SA, Faramarzi S, Mafi M, Ranjbar SF, Motavalli Sofiani S. Proposing a Hydrogen Liquefaction Cycle for Geothermal Energy Storage in an Innovative Multi-Generation System. Hydrogen, Fuel Cell & Energy Storage. 2025;12(1):1-8.

[10] Awad M, Said A, Saad MH, Farouk A, Mahmoud MM, Alshammari MS, et al. A review of water electrolysis for green hydrogen generation considering PV/wind/hybrid/hydropower/geothermal/tidal and wave/biogas energy systems, economic analysis, and its application. Alexandria Engineering Journal. 2024;87:213-39.

[11] Bi Y, Yin L, He T, Ju Y. Optimization and analysis of a novel hydrogen liquefaction process for circulating hydrogen refrigeration. international journal of hydrogen energy. 2022;47(1):348-64.

[12] Nedaei M, Keykhah A, Kamary B, Assareh E. Optimization and performance analysis of a geothermal-based power generation system based on flash-binary and dual-pressure evaporation organic Rankine cycles using zeotropic mixtures. Advances in Engineering and Intelligence Systems. 2023;2(03):61-75.

[13] Cao Y, Dhahad HA, Togun H, El-Shafay A, Alamri S, Rajhi AA, et al. Development and transient performance analysis of a decentralized grid-connected smart energy system based on hybrid solar-geothermal resources; Techno-economic evaluation. Sustainable Cities and Society. 2022;76:103425.

[14] Mehrpooya M, Sadaghiani MS, Hedayat N. A novel integrated hydrogen and natural gas liquefaction process using two multistage mixed refrigerant refrigeration systems. International journal of energy research. 2020;44(3):1636-53.

[15] Zhao X, Mu H, Li N, Shi X, Chen C, Wang H. Optimization and analysis of an integrated energy system based on wind power utilization and on-site hydrogen refueling station. International journal of hydrogen energy. 2023;48(57):21531-43.

[16] Seyam S, Dincer I, Agelin-Chaab M. Analysis of a clean hydrogen liquefaction plant integrated with a geothermal system. Journal of cleaner production. 2020;243:118562.

[17] Nouri M, Miansari M, Ghorbani B. Exergy and economic analyses of a novel hybrid structure for simultaneous production of liquid hydrogen and carbon dioxide using photovoltaic and electrolyzer systems. Journal of cleaner production. 2020;259:120862.

[18] Chang HM, Kim BH, Choi B. Hydrogen liquefaction process with Brayton refrigeration cycle to utilize the cold energy of LNG. Cryogenics. 2020;108:103093.

[19] Tekkanat B, Yuksel YE, Ozturk M. The evaluation of hydrogen production via a geothermal-based multigeneration system with 3E analysis and multi-objective optimization. International Journal of Hydrogen Energy. 2023;48(22):8002-21.

[20] Liu X, Hu G, Zeng Z. Performance characterization and multi-objective optimization of integrating a biomass-fueled brayton cycle, a kalina cycle, and an organic rankine cycle with a claude hydrogen liquefaction cycle. Energy. 2023;263:125535.

[21] Yilmaz C, Kanoglu M, Abusoglu A. Exergetic cost evaluation of hydrogen production powered by combined flash-binary geothermal power plant. International journal of hydrogen energy. 2015;40(40):14021-30.

[22] Sun Z, Lai J, Wang S, Wang T. Thermodynamic optimization and comparative study of different ORC configurations utilizing the exergies of LNG and low grade heat of different temperatures. Energy. 2018;147:688-700.

[23] Yuksel YE, Ozturk M, Dincer I. Energetic and exergetic performance evaluations of a geothermal power plant based integrated system for hydrogen production. International Journal of Hydrogen Energy. 2018;43(1):78-90.

[24] Ni M, Leung MK, Leung DY. Energy and exergy analysis of hydrogen production by a proton exchange membrane (PEM) electrolyzer plant. Energy conversion and management. 2008;49(10):2748-56.

[25] Boyaghchi FA, Chavoshi M, Sabeti V. Multi-generation system incorporated with PEM electrolyzer and dual ORC based on biomass gasification waste heat recovery: Exergetic, economic and environmental impact optimizations. Energy. 2018;145:38-51.

[26] Kianfard H, Khalilarya S, Jafarmadar S. Exergy and exergoeconomic evaluation of hydrogen and distilled water production via combination of PEM electrolyzer, RO desalination unit and geothermal driven dual fluid ORC. Energy conversion and management. 2018;177:339-49.

[27] Tsatsaronis G. Definitions and nomenclature in exergy analysis and exergoeconomics. Energy. 2007;32(4):249-53.

[28] Sayyaadi H. Multi-objective approach in thermoenvironomic optimization of a benchmark cogeneration system. Applied Energy. 2009;86(6):867-79.

[29] Wang L, Bu X, Wang H, Ma Z, Ma W, Li H. Thermoeconomic evaluation and optimization of LiBr-H2O double absorption heat transformer driven by flat plate collector. Energy Conversion and Management. 2018;162:66-76.

[30] Razmi AR, Janbaz M. Exergoeconomic assessment with reliability consideration of a green cogeneration system based on compressed air energy storage (CAES). Energy Conversion and Management. 2020;204:112320.

[31] Bejan A, Tsatsaronis G, Moran MJ. Thermal design and optimization. John Wiley & Sons; 1995.

[32] Kianfard H, Khalilarya S, Jafarmadar S. Exergy and exergoeconomic evaluation of hydrogen and distilled water production via combination of PEM electrolyzer, RO desalination unit and geothermal driven dual fluid ORC. Energy conversion and management. 2018;177:339-49.

[33] Akrami E, Chitsaz A, Nami H, Mahmoudi S. Energetic and exergoeconomic assessment of a multigeneration energy system based on indirect use of geothermal energy. Energy. 2017;124:625-39.

[34] Arora A, Kaushik S. Theoretical analysis of LiBr/H2O absorption refrigeration systems. International Journal of Energy Research. 2009;33(15):1321-40.

[35] Alirahmi SM, Rostami M, Farajollahi AH. Multicriteria design optimization and thermodynamic analysis of a novel multi-generation energy system for hydrogen, cooling, heating, power, and freshwater. International journal of hydrogen energy. 2020;45(30):15047-62.

[36] Emadi MA, Mahmoudimehr J. Modeling and thermo-economic optimization of a new multigeneration system with geothermal heat source and LNG heat sink. Energy Conversion and Management. 2019;189:153-66.